Caving-induced Subsidence Behaviour of Lift 1 at the Palabora Block Cave Mine

D P Sainsbury[1], B L Sainsbury[2], H-D Paetzold[3], P Lourens[4] and A Vakili[5]

ABSTRACT

The cave propagation behaviour of a jointed rock mass is strongly governed by the unique nature of joints and discontinuities, together with the intact strength of rock bridges that make up the rock fabric. A discrete finite difference (DFD) modelling technique has been developed to allow for the detailed consideration of the rock mass structural fabric at many scales and through many different stress paths that can be used for complex mine-scale analysis. The DFD methodology uses interfaces to explicitly represent large-scale structures and ubiquitous joints embedded within the simulated rock mass matrix to characterise intermediate structures. Through simulated testing of DFD materials, properties such as strength anisotropy and scale effects can be obtained. This paper discusses the successful application of implementing a DFD modelling technique for the back-analysis of caving-induced subsidence behaviour of Lift 1 at the Palabora mine.

INTRODUCTION

The Palabora copper mine is a large, 32 000 t/d block cave operation located in the eastern half of Limpopo, South Africa's northern-most province. Palabora Mining Company is currently developing a second lift (Lift 2) in addition to their existing block cave operation (Lift 1).

Upon breakthrough of the Lift 1 cave to the base of the open pit in 2004, significant instability in the north wall of the open pit occurred. Multiple numerical modelling studies have been conducted since this time to investigate the north wall failure and the associated subsidence (Brummer, Li and Moss, 2006; Sainsbury, Pierce and Mas Ivars, 2008; Vyazmensky *et al*, 2010; Woo *et al*, 2012). None of the published analyses have fully captured the three-dimensional evolution of the cave propagation, crown pillar failure/breakthrough, slope failure and surface cracking formation beyond the crest of the pit.

To provide confidence in the prediction of caving-induced subsidence associated with the development of Lift 2, detailed three-dimensional numerical modelling has been conducted with a hybrid Abaqus/CAE-FLAC3D discrete finite difference (DFD) modelling approach. The approach has been able to accurately simulate the evolution of the north wall failure from cave initiation through to the existing subsidence zone of influence magnitude and geometry.

BACKGROUND

Mining geometry

The Palabora mine began as an open cut copper operation in 1964. Production commenced in 1966 at a rate of 30 000 t/d, increasing to 82 000 t/d prior to closure in 2002. The final dimensions of the pit are 800 m deep and 1650 m to 1900 m in diameter.

Underground block cave mining commenced in April 2001. The Lift 1 Undercut Level is located 1200 m below the surface and 420 m below the pit floor. Upon breakthrough of the Lift 1 cave to the base of the open pit in 2004, cracking was observed in the north-west wall. Cracking evolved over several months into major movements and eventually failure of the pit wall. The failure extended 300 m beyond the pit crest, affecting access, haul roads, tailings dams, water and power lines, water reservoirs and a railway line. Figure 1 presents the existing mine geometry and surrounding infrastructure.

A view of the evolution of the north wall failure in the pit is provided in Figure 2 and a summary of the Lift 1 cave progression is provided as follows:

- *Second quarter (April) 2002.* Self-sustaining cave propagation initiates when the mining footprint hydraulic radius (HR) reaches 45 m (Moss, Diachenko and Townsend, 2006). This is approximately 30 per cent greater than the predicted size, but is still significantly smaller than the

1. MAusIMM, Principal Rock Mechanics Engineer, Mining One Consultants, Melbourne Vic 3000. Email: dsainsbury@miningone.com.au
2. MAusIMM, Associate Professor, Monash University, Clayton Vic 3800. Email: bre-anne.sainsbury@monash.edu
3. Package Manager, Growth Division, Palabora Copper (Pty) Limited, Phalaborwa, South Africa. Email: hans.paetzold@palabora.co.za
4. Geotechnical Superintendent, Vertical Development and Geotechnical, Growth Division, Palabora Copper (Pty) Limited, Phalaborwa, South Africa. Email: paulien.lourens@palabora.co.za
5. MAusIMM(CP), Senior Rock Mechanics Engineer, Mining One Consultants, Melbourne Vic 3000. Email: avakili@miningone.com.au

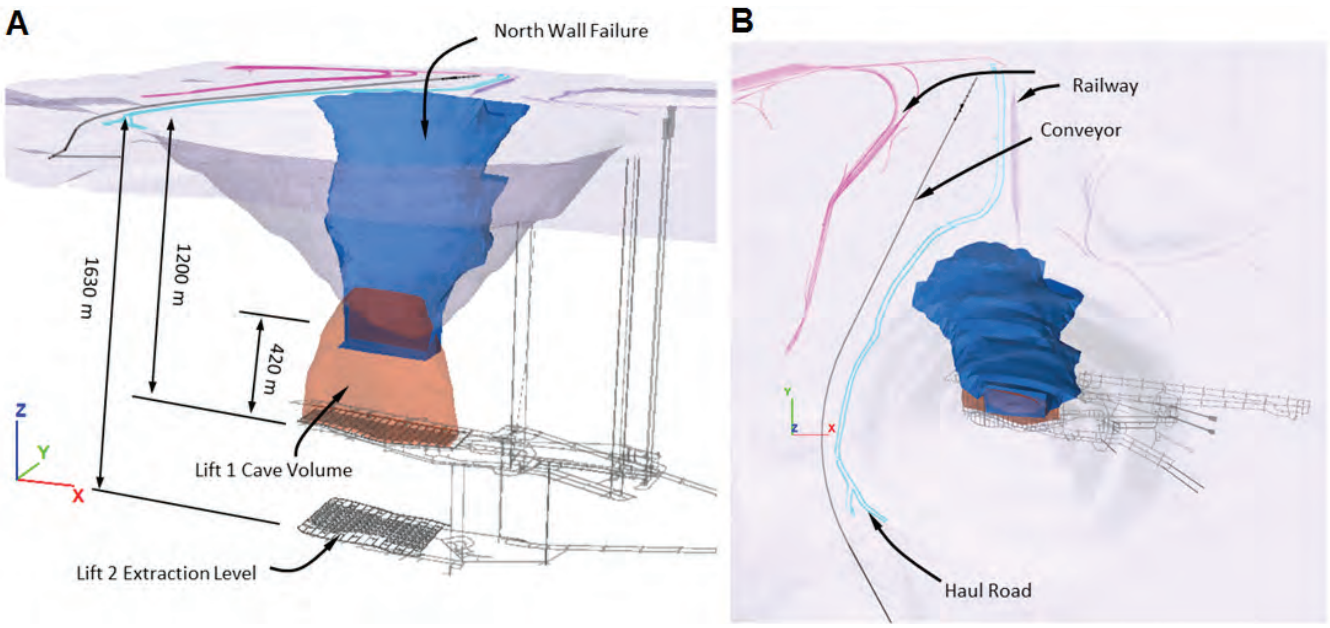

FIG 1 – Palabora mine geometry: (A) isometric view; and (B) plan view.

FIG 2 – Evolution of the north wall failure (looking north-west).

total footprint HR of approximately 90 m. The location and magnitude of seismic events recorded during the early stages of production suggest that the yield zone (or aseismic zone) extended approximately 55–83 m beyond the mobilised zone (Sainsbury, 2012).

- *Fourth quarter 2003.* The crown pillar yields (becomes aseismic), driving seismicity beneath the Lift 1 Extraction Level (Glazer and Hepworth, 2006).
- *First quarter 2004.* The mobilised zone intersects the pit floor after production ramps up to an average rate of draw of 116 mm (Moss, Diachenko and Townsend, 2006). Movement of the pit walls increased substantially upon cave breakthrough into the bottom of the pit. The greatest amount of movement occurred in the north wall, where displacements of in excess of 1.5 m were measured over a year (Moss, Diachenko and Townsend, 2006; Figure 2a).
- *Fourth quarter 2004.* North wall pit slope failure. The first indication of large-scale instability was observed when a bench failure adjacent to one of the pit sumps resulted in the development of tension cracks approximately 250 m beyond the north-west crest of the pit. The failure continued to grow in size over a period of 18 months until it encompassed a major section of the north wall extending 50 m beyond the pit crest and down to the original pit floor. Approximately 100 Mt was mobilised in this failure, which was approximately 800 m high by 300 m wide (Moss, Diachenko and Townsend, 2006; Figure 2d).
- *First quarter 2015.* Inspection of the current failure scarp reveals significant structural control on the failure mechanism and the subsidence zone of influence. Mass sliding of the failure volume can be observed bounded by large-scale structures that form a north-north-west structural orientation (NNWSO) (Figure 3).

Previous numerical modelling studies

Multiple numerical modelling studies have been conducted to investigate the north wall failure and the associated caving-induced surface subsidence at Palabora (Brummer, Li and Moss, 2006; Sainsbury, Pierce and Mas Ivars, 2008; Vyazmensky *et al*, 2010; Woo *et al*, 2012). However, none of the published analyses conducted to date have fully captured the three-dimensional evolution of the cave propagation, crown pillar failure/breakthrough, slope failure and surface cracking formation.

An initial forensic review of the geotechnical conditions associated with the north wall failure was performed by Brummer, Li and Moss (2006) using the three-dimensional distinct element code 3DEC (by Itasca Consulting Group). The conceptual modelling suggested that the failure was most likely caused by a series of weak, persistent joint structures forming large-scale wedges that let daylight into the Lift 1 cave void. The model did not account for NNWSO. The simulated deep-seated failure mechanism is illustrated in Figure 4a. Subsequent mass balance and grade reconciliation, together with monitoring of the active failure scarp, have shown that the observed failure mechanism is relatively shallow (ie no greater than 50 m deep within the pit), which does not match with the model results.

A more thorough consideration of the rock mass joint fabric was conducted in the two-dimensional hybrid finite element/discrete element code ELFEN (by Rockfield) by Vyazmensky *et al* (2010). Although, limited to two dimensions and without the simulation of the large-scale fault structures, the analyses showed how the north wall failure could develop. The numerical modelling approach simulated a complex north wall failure mechanism that was primarily governed by a combination of slip along joints and brittle intact rock failure combining in a step-path failure surface (Figure 4b).

Sainsbury, Pierce and Mas Ivars (2008) extended the simulation of the rock mass joint fabric within the north wall to three dimensions using a ubiquitous jointed rock mass modelling technique (Sainsbury, 2012). The evolution of the cave volume was accurately simulated based on the actual production draw history rather than deleting a vertical column of rock immediately above the mining footprint. The model was able to accurately capture the cave propagation behaviour, crown pillar failure/breakthrough and initiation of the north wall failure (Figure 4c). However, the model was not able to accurately simulate propagation of the failure over the full pit slope height or the subsequent subsidence zone of influence beyond the crest.

Woo *et al* (2012) conducted a series of analyses within the three-dimensional finite difference code FLAC3D, version 5.01 (by Itasca Consulting Group), primarily to calibrate subsidence displacements with high-resolution interferometric synthetic aperture radar (InSAR) data. The simplified model did not include large-scale structures or the simulation of the rock mass joint fabric. In addition, rather than simulating the evolution of the cave volume based on the production draw schedule, the analyses imposed a predefined cave volume into the model. Although elevated slope displacements were simulated in the vicinity of the north wall failure (100 mm), as illustrated in Figure 4d, this model was unable to simulate the north wall failure as emergent behaviour.

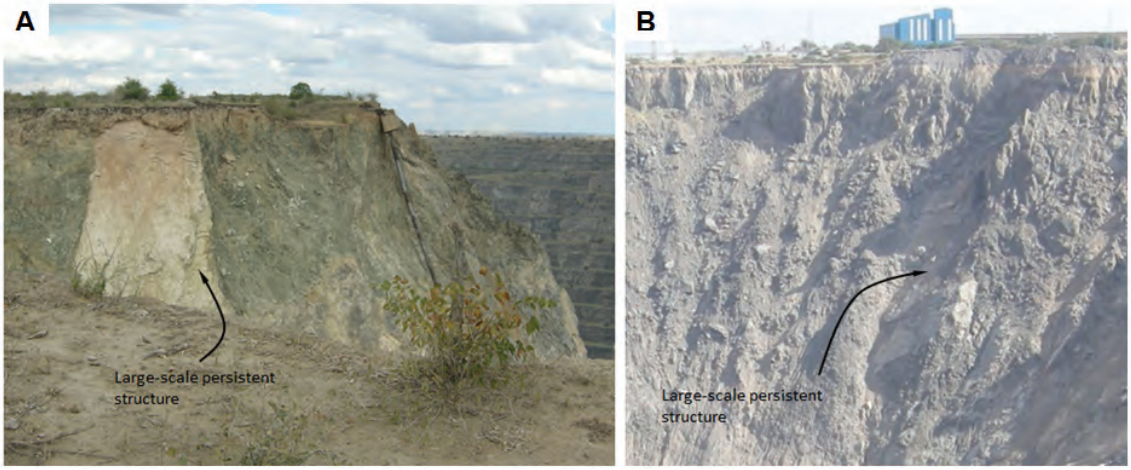

FIG 3 – Current day failure scarp at the crest of the pit.

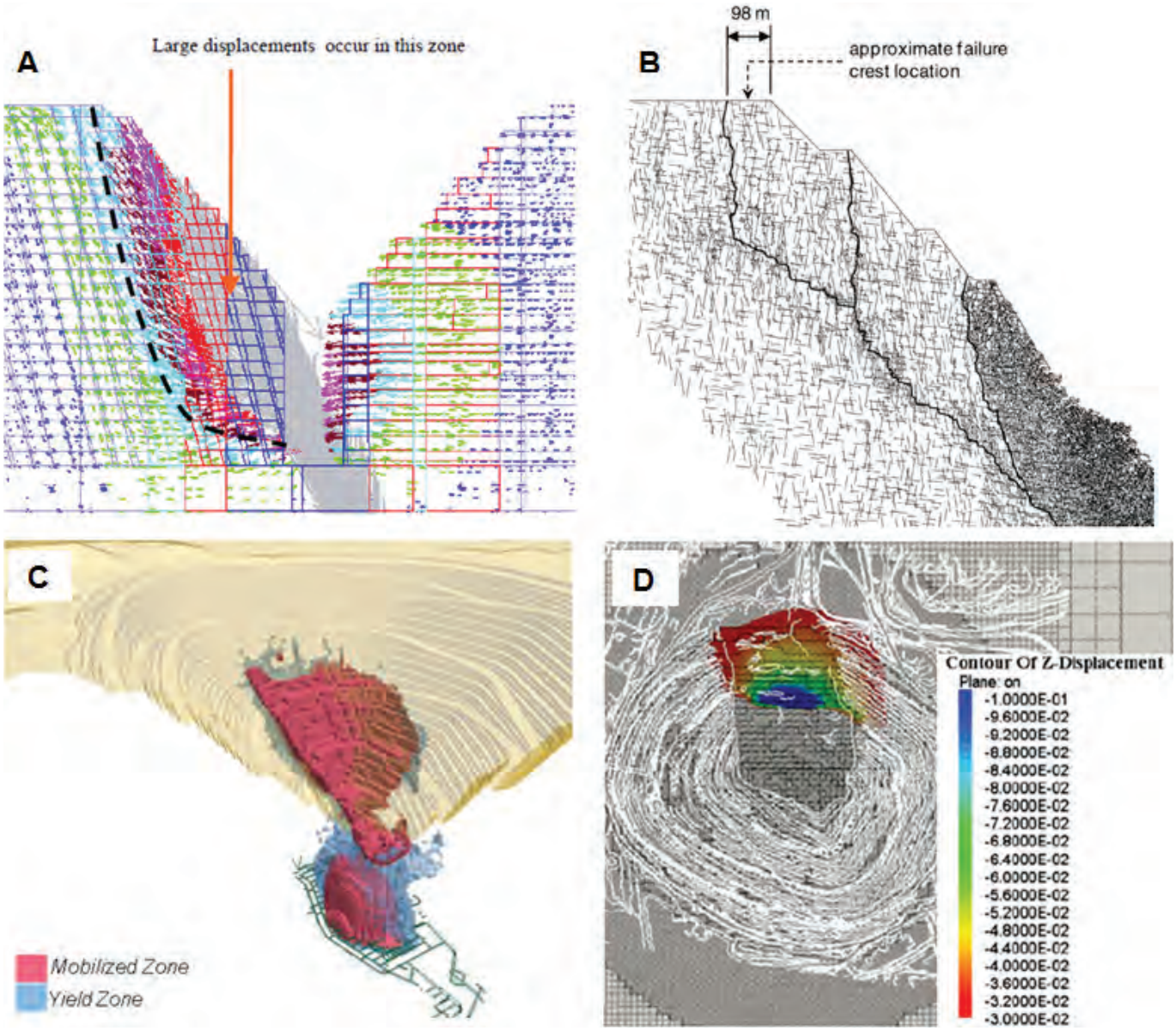

FIG 4 – Numerical analyses of the Palabora north wall failure. (A) Brummer, Li and Moss, 2006; (B) Vyazmensky *et al,* 2010; (C) Woo *et al,* 2012; (D) Sainsbury *et al,* 2008.

NUMERICAL ANALYSIS OF THE NORTH WALL FAILURE

Modelling methodology

In order to provide a more accurate assessment of the north wall failure and associated caving-induced subsidence, a hybrid Abaqus/CAE (by Dassault Systemes)–FLAC3D, DFD modelling approach has been developed. The modelling approach uses the advanced mesh generation capabilities of Abaqus/CAE together with the finite difference calculation and advanced constitutive models of FLAC3D.

Figure 5 illustrates the high-quality model discretisation achieved with the Abaqus/CAE–FLAC3D model construction approach. The hybrid DFD model allows discrete simulation of the large-scale structure and ubiquitous joint simulation of intermediate-scale structures. The rock mass material in between the structures is simulated as a continuum with a strain softening, dilatant constitutive model based on the Hoek–Brown failure criteria.

Production draw within the model has been simulated by using the industry reviewed and validated algorithms developed by Sainsbury (2012). Through these algorithms, the cave and subsidence profile is able to develop based on the specified draw strategy, evolving induced stress conditions and the simulated constitutive behaviour of the rock mass. In doing so, hang-ups, overbreaks and rapid advance rates can all be predicted as emergent behaviour with direct correlation to a mass-based production draw schedule.

Geotechnical domains

The geotechnical domains at Palabora have been defined by lithological boundaries. Based on geological mapping, five main lithological units occur, including banded carbonitite (BCB), transverse carbonitite (TCB) and foskorite (FOS). The BCB and FOS have a generally concentric arrangement with TCB at the centre. The central core is surrounded by micaceous pyroxenite (MPY) that is intersected by dolerite dykes trending NE–SW, as shown in Figure 6a.

In situ stress

There is high uncertainty associated with the magnitude and orientation of the *in situ* stress regime at the Palabora mine. Previous stress testing studies and numerical calibrations of existing conditions have resulted in significant variation in the principal stress magnitudes. The orientation of the

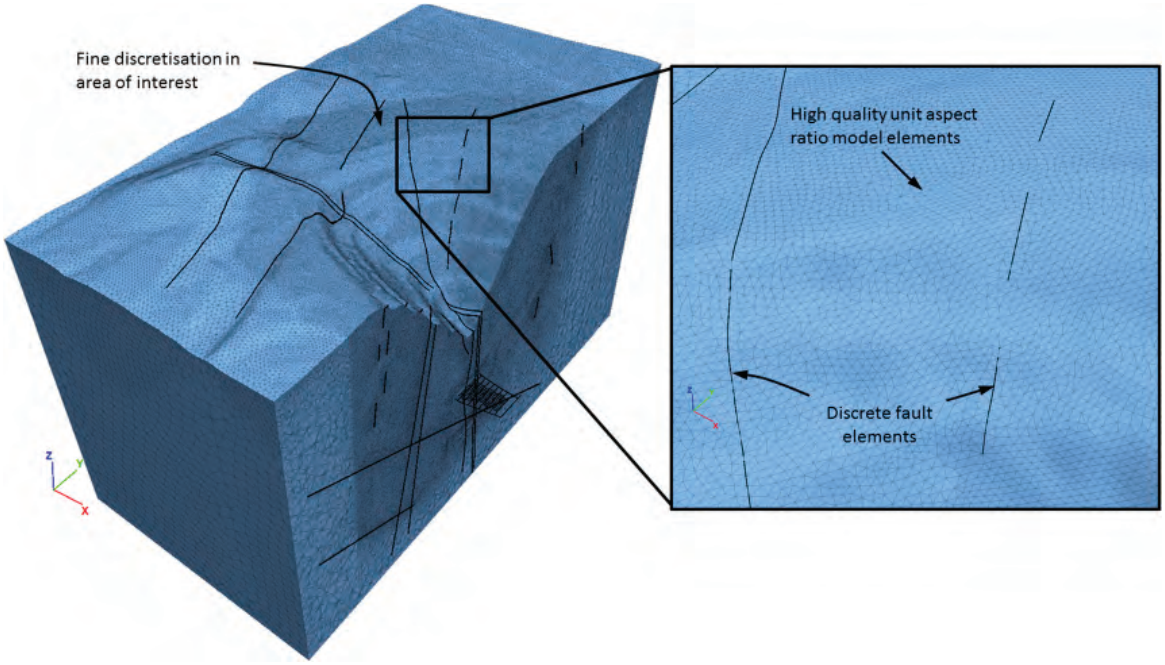

FIG 5 – Model discretisation.

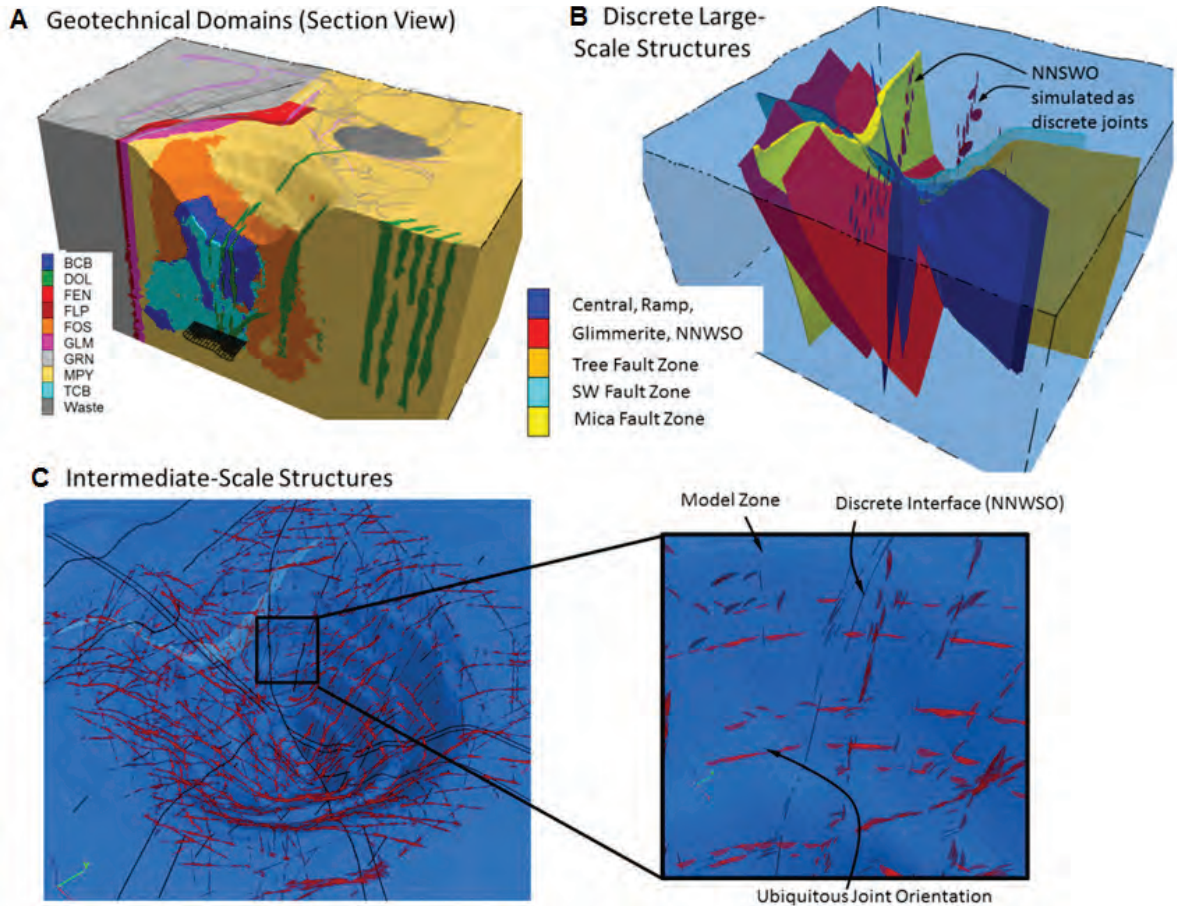

FIG 6 – Model geometry. (A) Geotechnical domains; (B) large-scale explicit fault structures; (C) intermediate-scale structures simulated as ubiquitous joints within the model (red) embedded within a rock mass matrix (blue).

principal stress direction has been measured at orientations between 000° and 340°.

Previous analyses of cave propagation and subsidence at Palabora (Sainsbury, Pierce and Mas Ivars, 2008) have used an *in situ* stress regime with a horizontal to vertical stress ratio of 2:1. This *in situ* stress regime was selected based on a sensitivity analysis of the existing north wall slope failure. However, after review of the limited stress-induced damage observed throughout the Lift 1 infrastructure and initial Lift 2 development, a revised lower *in situ* stress regime with a horizontal to vertical stress ratio of 1.2:1 has been adopted for the current analysis. This stress magnitude is consistent with a stress assessment provided by Gash (1999) at the site.

Rock mass properties

A numerical model that represents the caving process must account for the progressive failure and disintegration of the rock mass from intact/jointed to a caved material. In this complex process, creation of the cave results in:

- deformation and stress redistribution of the rock mass above the undercut
- failure of the rock mass in advance of the cave, with an associated progressive reduction in strength from peak to residual levels
- dilation, bulking, fragmentation and mobilisation of the caved material.

This overall process – loading of the rock mass to its peak strength, followed by post-peak reduction in strength to some residual level with increasing strain – is often termed a 'strain softening' process and is the result of strain-dependent material properties.

In the caving model applied herein, the strain-softening material is described by bi-linear, Mohr–Coulomb failure criteria in which the post-peak strength behaviour is a function of plastic shear strain-dependent rock mass cohesion and friction angle. The plastic shear strain required in going from peak strength to a fragmented rock mass defines the brittleness of the failure. The residual (bulked) rock mass strength properties used included cohesion of 0 MPa, tension of 0 MPa and friction of 43°. These properties are progressively reached through strain-dependant softening relationships.

The median rock mass strength and deformation parameters used to simulate the peak strength for each of the geotechnical domains are presented in Table 1. The material properties for the GRN, FEN, FLP and GLM domains in Table 1, which lie outside of the cave footprint, were obtained from a summary of material properties compiled by Woo *et al* (2012).

The plastic shear strain required to progress from peak strength to a completely fragmented rock mass defines the brittleness of the rock mass failure and can be related to the geological strength index (GSI) of the material. Equation 1 has previously been used to estimate the FLAC3D critical strain parameter (ϵ^{ps}_{crit}) for each of the rock mass domains. Δz represents the zone size.

$$\epsilon^{ps}_{crit} = (-0.0142\ GSI + 1.3967) / \Delta z \quad [1]$$

The relationship has been developed based on six case histories (Sainsbury, 2012). Comparison of the rock mass responses using this equation compare well with synthetic rock mass modelling results for Palabora rock mass domains (Sainsbury, Pierce and Mas Ivars, 2008).

Large-scale structures

The Palabora orebody contains at least five major structures: Central Fault Zone (CFZ), South-west Fault Zone (SWFZ), Tree Fault Zone, Mica Fault Zone and a NNWSO. The NNWSO does not define discrete structures, but instead denotes a group of structures with this orientation that exist in a confined area of the pit (Figures 7 and 8).

A combination of interface structures with zero thickness that can slip and separate and zones with a specific thickness have been used to represent large-scale fault structures within the numerical model. Figure 6b illustrates the interfaces and zones used to simulate the structures in FLAC3D. The NNWSO has been simulated as a series of discrete disks with a diameter between 100 m and 200 m.

Average strength values of cohesion of 50 kPa and friction of 35° have been estimated for the structures based on a database compiled by Barton (1970). A tension value of 0 kPa has been assumed for the structures. These values are consistent with the joint properties derived for the rock mass and have been developed based on sensitivity analysis and large-scale calibration to the existing conditions (Sainsbury, Pierce and Mas Ivars, 2008). The joint normal and shear stiffness have both been estimated at 10 GPa/m and 1 GPa/m respectively, based on the stiffness of the rock mass.

Intermediate-scale structures

The BCB, TCB, FOS and MPY geotechnical domains are all characterised by low fracture frequency and large fracture persistence. Figure 9 illustrates an example of persistent joints exposed in the north-east wall of the pit within the MPY domain.

Mas Ivars *et al* (2008) developed a series of discrete fracture networks (DFNs) for the geotechnical domains at Palabora. The DFN generation procedure was based on a representative elemental volume of 100 m and included the results of both underground and open pit scanline mapping. The joint orientations of the carbonatite domain are presented in Figures 10a and 10b. Figures 10c and 10d illustrate the resulting DFN and joint orientations simulated in the analysis.

In order to simulate the effect of the persistent intermediate-scale joint fabric, the DFNs created for each Palabora domain have been filtered to remove joints with a persistence of less than 60 m. Figure 11 illustrates the resulting DFNs that represent the intermediate-scale structures within each

TABLE 1

Median peak strength rock mass material properties.

Domain	Density(kg/m³)	Geological strength index	σ_{ci} (MPa)	m_i	E_{rm}(GPa)	v
GRN	3100	75	300	31.0	73.0	0.21
FEN	3100	70	200	16.0	44.7	0.23
FLP	3100	54	80	16.0	11.0	0.24
GLM	3100	50	37	6.0	8.1	0.25
BCB	2865	73	114	17.2	40.1	0.21
TCB	2887	73	110	16.9	39.4	0.21
DOL	3055	73	277	21.7	62.4	0.21
FOS	3530	74	93	15.2	38.4	0.21
MPY	3037	76	78	10.2	39.5	0.20
Fault	2750	35	100	15.0	5.0	0.26

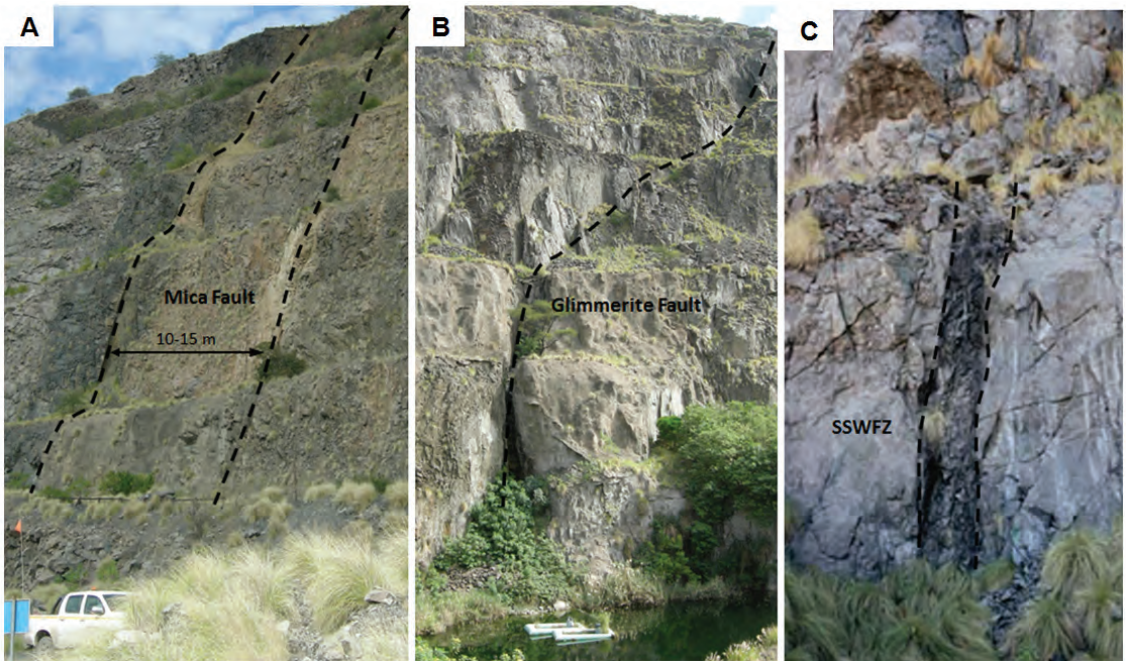

FIG 7 – Exposure of the Mica Fault, Glimmerite Fault and South-west Fault Zone within the open pit.

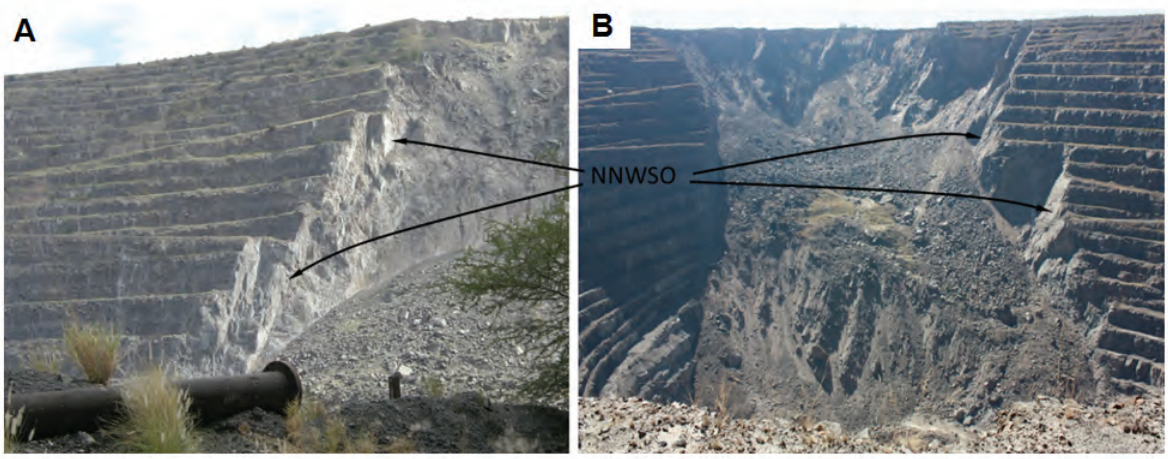

FIG 8 – Exposure of north-north-west structural orientation in the north wall failure scarp.

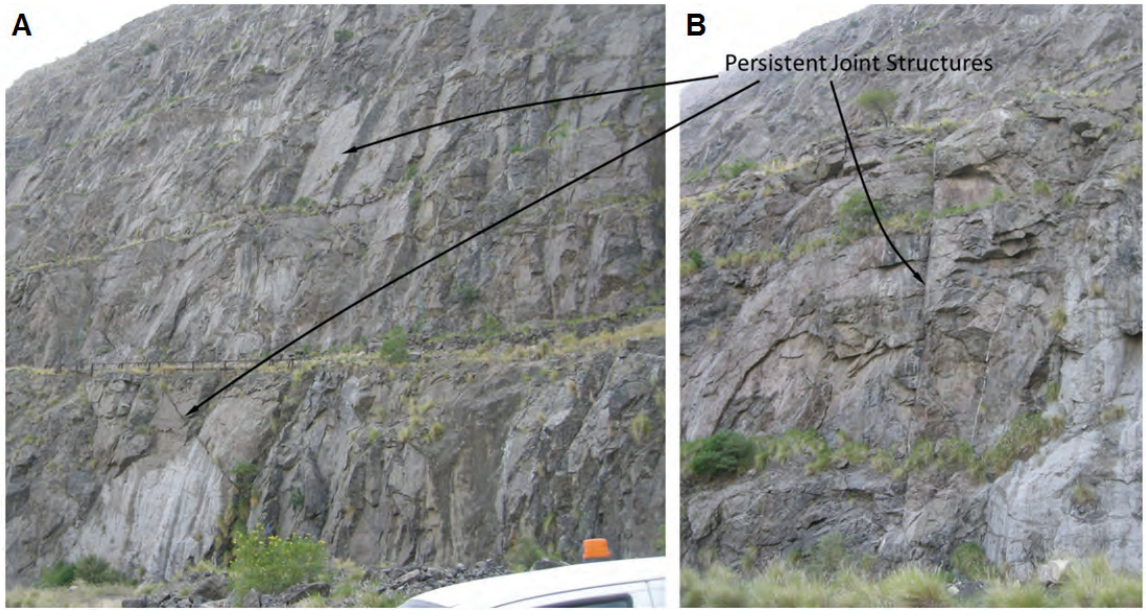

FIG 9 – Intermediate-scale structures within the micaceous pyroxenite domain.

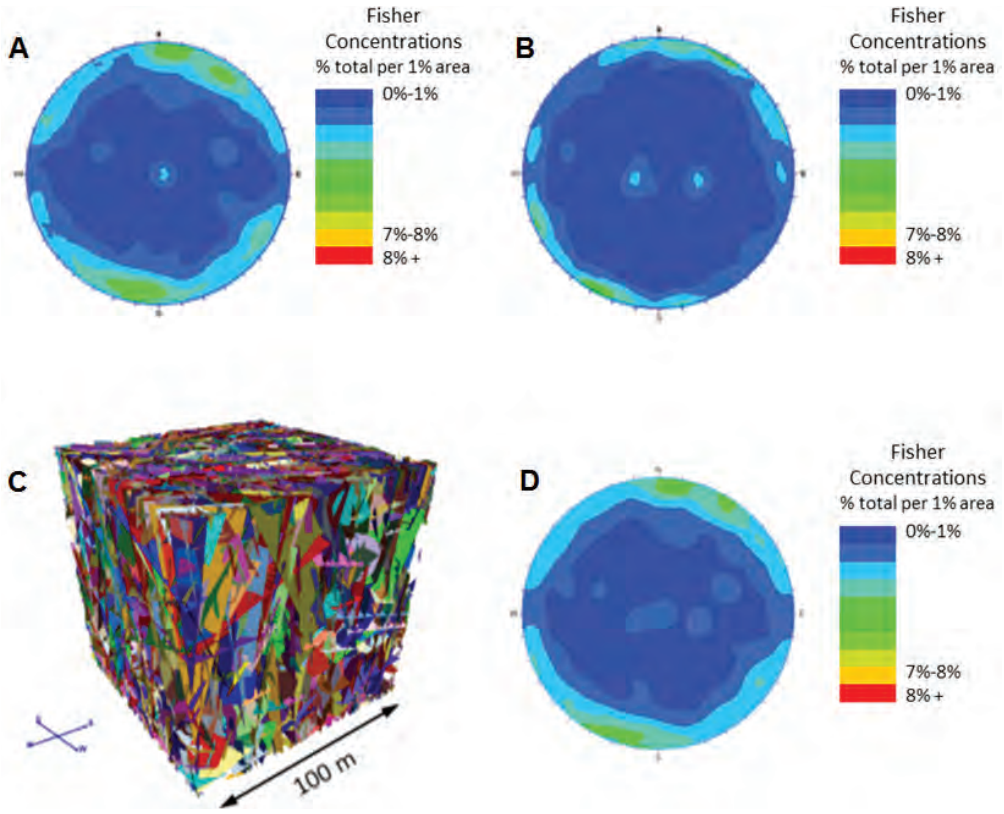

FIG 10 – Joint orientations and discrete fracture network (DFN) of the carbonatite domain from: (A) underground scanline mapping; (B) open pit mapping; (C) DFN; and (D) DFN joint orientations.

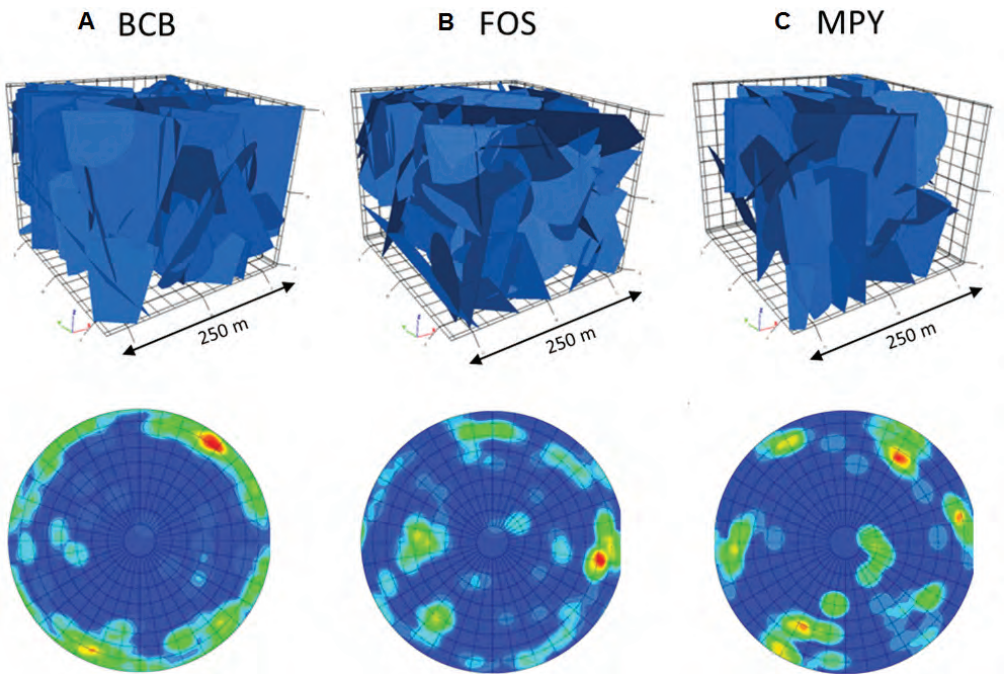

FIG 11 – Filtered discrete fracture networks used to simulate persistent joint structure.

domain. Figure 6c illustrates the intermediate-scale structures that have been simulated as ubiquitous joint elements in the numerical model of Palabora.

SIMULATION OF THE NORTH WALL FAILURE

Simulation of pit slope stability

Prior to underground mining from the Lift 1 Extraction Level, open pit mining has been simulated in the model to ensure that a representative stress path is induced within the cave column. Simulation of open pit mining has been conducted through the systematic removal of rock mass benches within the open pit shell from the ground surface down to the final pit limits (approximately -420 mRL).

Du Plessis and Martin (1991) reported that all slopes developed during excavation of the Palabora pit performed well, with only local slope flattening and reinforcement required to achieve stable slopes in the vicinity of some of the

fault structures. Figure 12 illustrates a comparison between measured displacements along the crest of the pit between 1984 and 1990 and model displacement simulated over the same time period. A good correlation between the measured slope relaxation and the model displacement response is achieved. Local slope instability in the vicinity of the Mica Fault can be observed in the model (Figure 12b).

Figure 13 illustrates the slope response at the completion of open pit mining in 2002. Local slope instability controlled by the CFZ and SWFZ can be observed in the base of the pit (Figures 13a and 13b). Local wedge-type failures associated with the NNWSO can also be observed (Figures 13c and 13d). The simulation results are consistent with the *in situ* observations during development.

Simulation of the Lift 1 cave propagation behaviour

Simulation of production draw from Lift 1 was conducted using the caving algorithm described by Sainsbury (2012). Figures 14 and 15 illustrate the evolution of the Lift 1 cave mobilised zone and the limit of large-scale cracking in the pit at the end of 2003 (prior to the north wall failure) and 2004 (after the north wall failure).

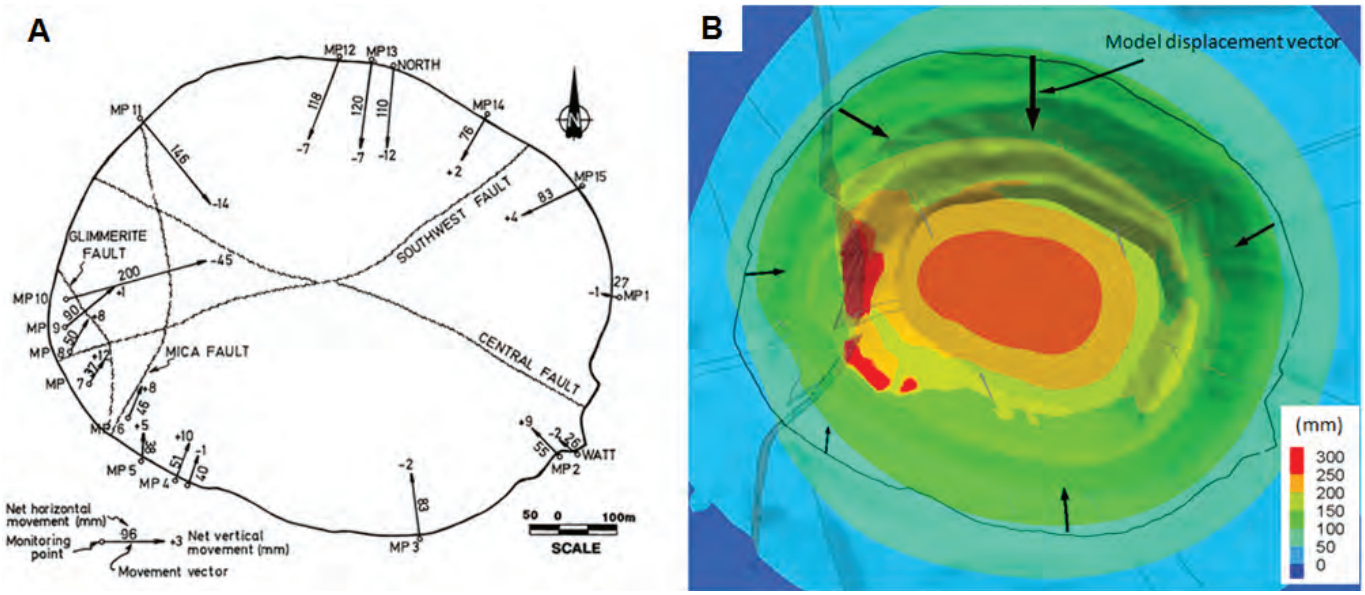

FIG 12 – (A) Pit displacements between 1984 and 1990 (after Du Plessis and Martin, 1991); (B) approximate model displacement increment between 1984 and 1990.

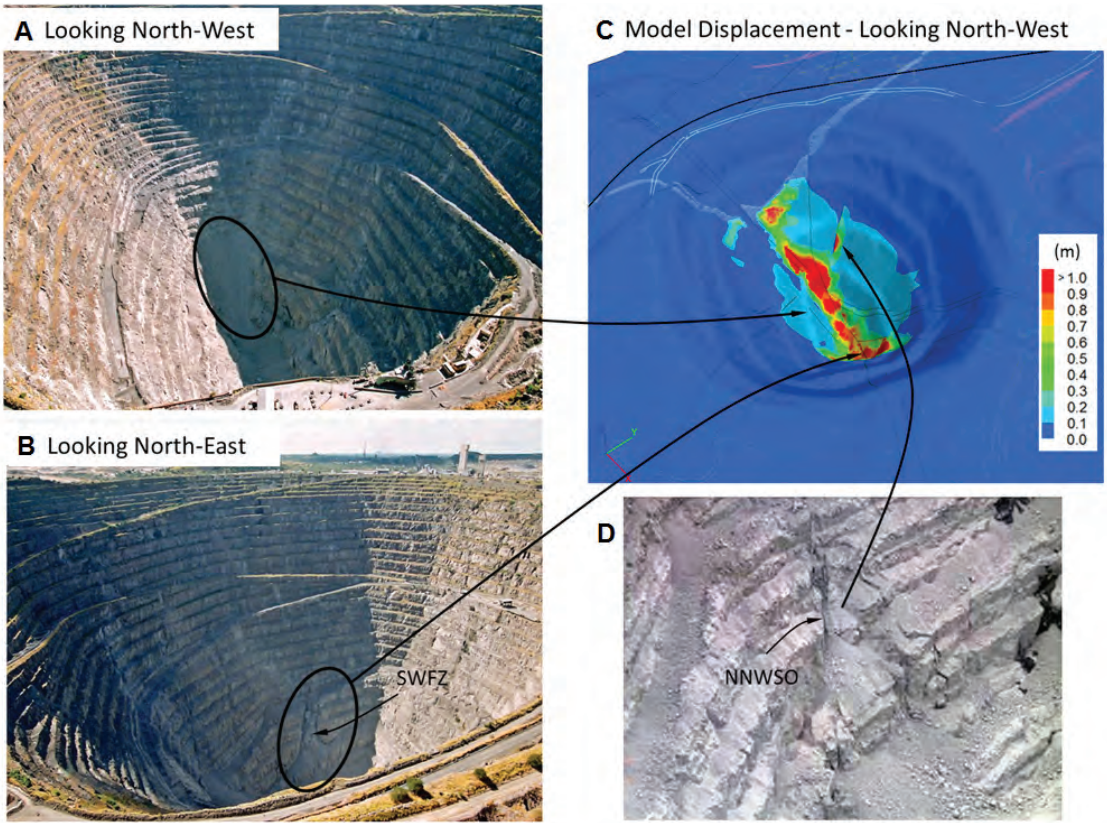

FIG 13 – Slope performance at the completion of open pit mining.

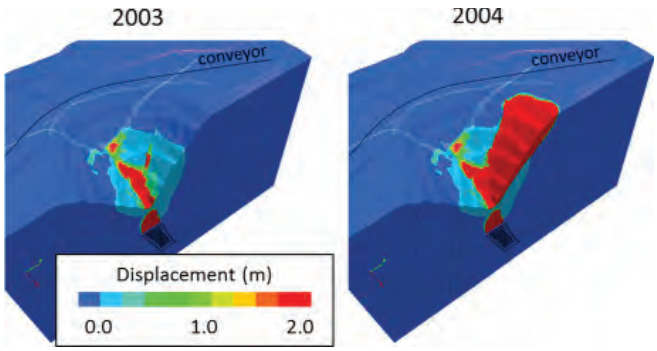

FIG 14 – Evolution of Lift 1 cave mobilised zone (displacement >2 m).

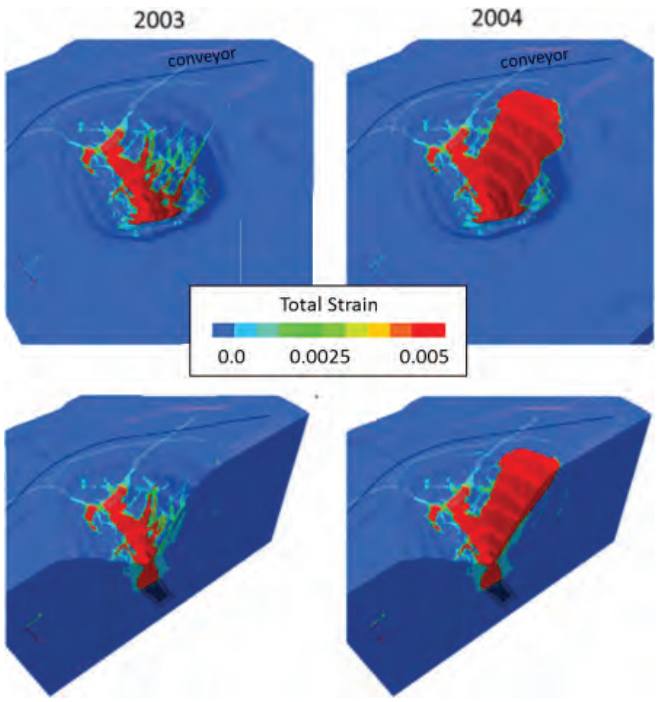

FIG 15 – Evolution of the Lift 1 limit of large-scale cracking (total strain >0.5 per cent).

The model accurately predicts the evolution of breakthrough of the Lift 1 cave to the base of the pit in 2003, followed by mobilisation of the north wall in 2004. Upon breakthrough of the Lift 1 yield zone (total strain >0.5 per cent) to the base of the pit in 2003, yielding associated with the NNWSO structures and loss of confinement at the toe of the slope is simulated to extend up the north wall. Complete mobilisation of the north wall bounded by the NNWSO structures is predicted during 2004.

Figure 16 illustrates a comparison of the simulated and best-estimate cave volume. Best-estimate cave volumes have been derived from mass balance and grade reconciliation models together with geotechnical monitoring around the active failure scarp. Due to the lateral constraint provided by the conical-shaped pit, the resulting mobilised zone within the north wall failure is predicted to be relatively shallow. The model results provide a good correlation with the best-estimate cave volume.

Simulation of the Lift 1 subsidence zone of influence

A total strain criterion of 0.005 (0.5 per cent) has been used to assess the limits of large-scale surface cracking beyond the crest of the north wall failure. This total strain criterion has previously been used to calibrate the limits of large-scale fracturing at the Kiruna (Sainsbury and Stockel, 2012), Grace (Sainsbury, Lorig and Sainsbury, 2010), Century (Sainsbury, Sainsbury and Sweeney, in press) and El Teniente (Cavieres *et al*, 2003) mines.

Figure 17 illustrates a plan view of the evolution of total strain predicted at the crest of the north wall slope. The area in red indicates total strain greater than 0.005 (0.5 per cent), which is likely to cause large-scale cracking in the rock mass. The limits of large-scale cracking predicted after simulation of mining until 2014 provides a close match to the limits of the failure scarp observed on-site at the end of 2014.

The Society of Mining Engineers (Singh, 1992; updated by Harrison, 2011) provide guidelines for the classification of damage to buildings from mining-induced subsidence caused by horizontal strain and angular distortion. Figure 18 illustrates the limit of continuous subsidence based on the building damage criteria developed by Harrison (2011). The damage criteria is consistent with the mapped tension cracks behind the main failure scarp that indicates slight to moderate building damage.

SUMMARY AND CONCLUSIONS

A hybrid DFD technique has been developed to reproduce the caving-induced slope failure mechanisms at the Palabora mine in South Africa. The numerical technique has been able to accurately simulate both the cave propagation and subsidence behaviour that have occurred during cave initiation, propagation, surface breakthrough and steady-state production draw. Through the use of robust subsidence criteria

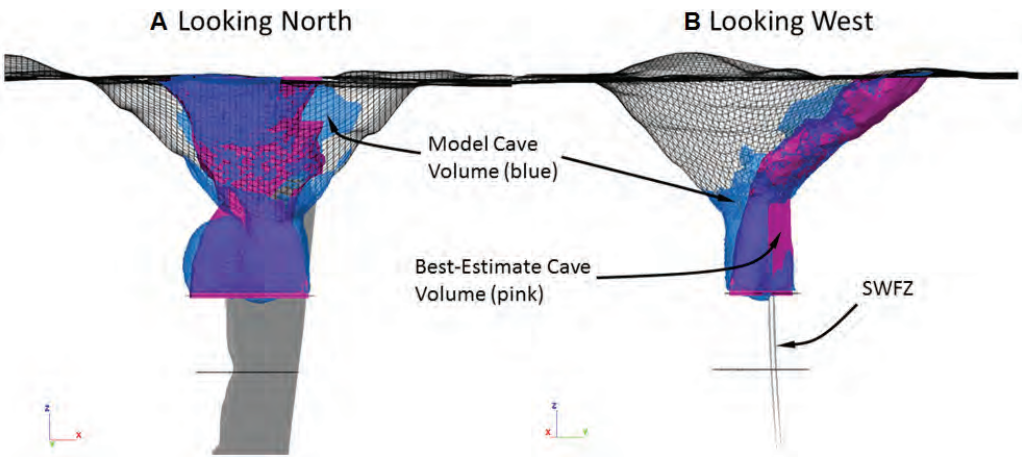

FIG 16 – Comparison of the simulated and best-estimate cave volume shapes after 2014.

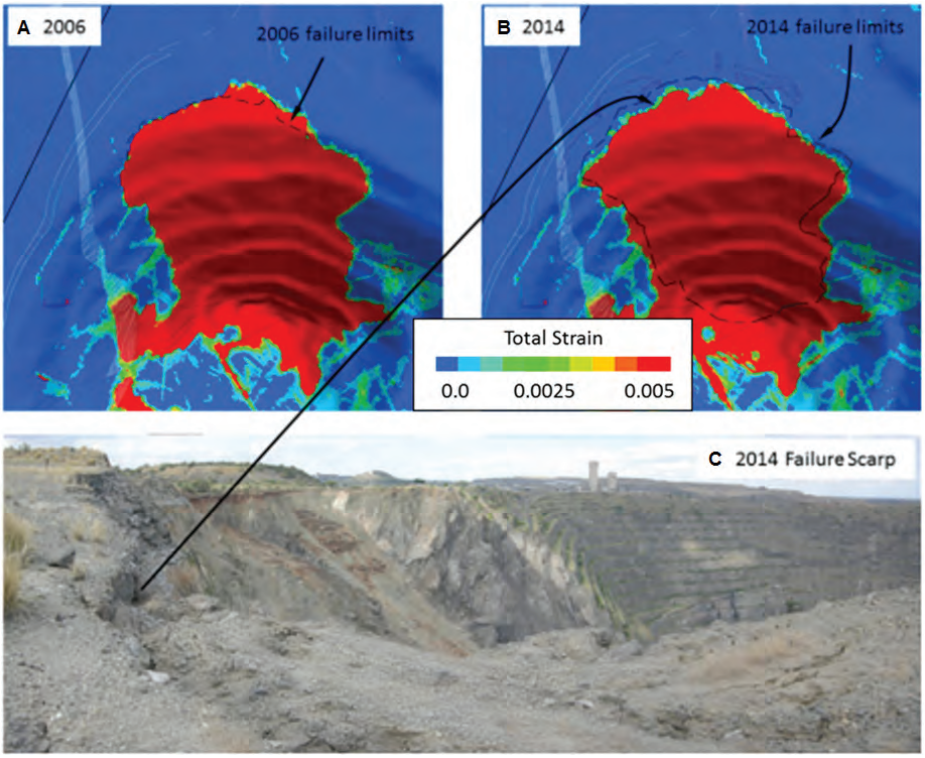

FIG 17 – Limit of large-scale cracking (total strain >0.5 per cent).

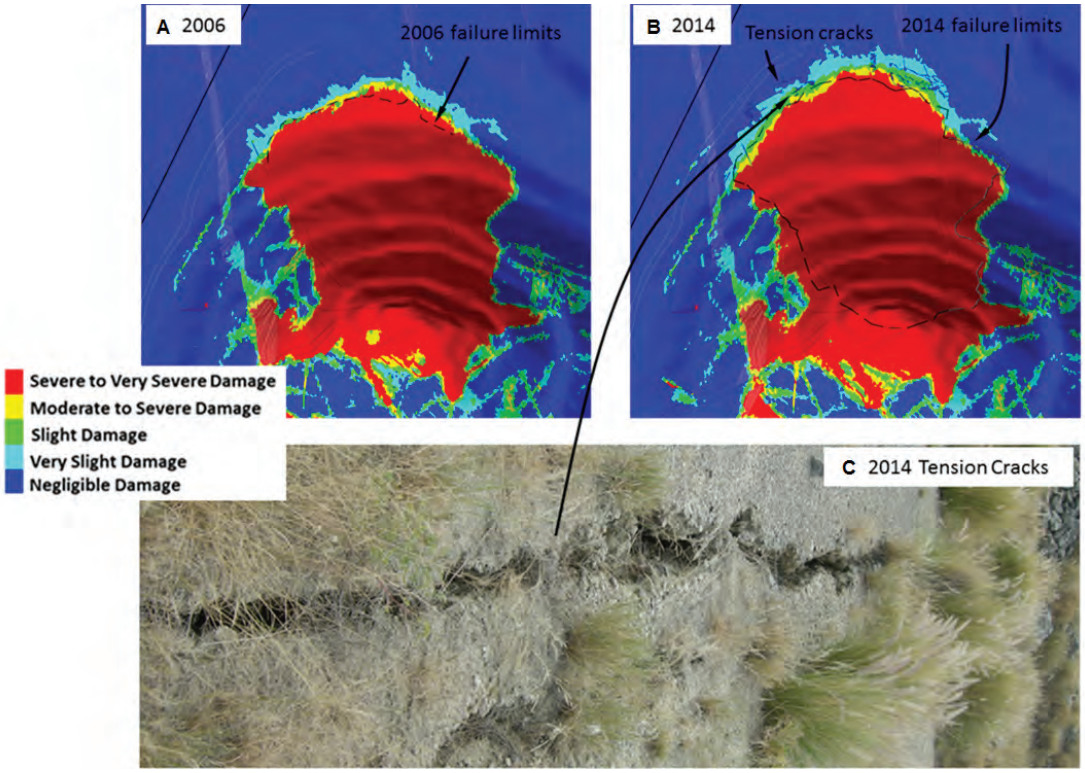

FIG 18 – Limit of continuous subsidence (Horizontal Strain and Angular Distortion Criteria, after Harrison, 2011).

that have been validated at a number of caving operations, the risk of mining-induced surface subsidence adversely affecting existing infrastructure beyond the pit crest at Palabora has been successfully managed through an iterative modelling approach. Through the use of accurate production draw algorithms and sophisticated hybrid DFN techniques, it is possible to predict these pit-cave interactions in the future and reduce the risk of unknown geotechnical conditions and/or interactions.

ACKNOWLEDGEMENTS

The authors wish to thank the management team at the Palabora mine for approval to publish this work.

REFERENCES

Barton, N, 1970. A low strength material for simulation of the mechanical properties of intact rock in rock mechanics models, in *Proceedings 2nd Congress International Society of Rock Mechanics*, pp 99–110 (International Society for Rock Mechanics: Lisbon).

Basson, I, Lourens, P, Paetzold, H and Thomas, D, 2015. The link between major structures and the Phalaborwa deposit: clues from structural analysis and 3D modelling.

Brummer, R, Li, H and Moss, A, 2006. The transition from open pit to underground mining: an unusual slope failure mechanism at Palabora, in *Proceedings International Symposium on Stability of Rock Slope in Open Pit Mining and Civil Engineering*, pp 411–420 (The South African Institution of Mining and Metallurgy: Johannesburg).

Cavieres, P, Gaete, S, Lorig, L and Gómez, P, 2003. Three-dimensional analysis of fracturing limits induced by large scale underground mining at El Teniente mine, in *Proceedings 39th US Rock Mechanics Symposium* (eds: P J Culligan, H H Einstein and A J Whittle), pp 893–900 (Verlag Glückauf: Essen).

Dassault Systemes, 2015. Abaqus/CAE. Vélizy-Villacoublay Cedex – France: Dassaut Systemes.

Du Plessis, L and Martin, D, 1991. Numerical modelling studies for the design of rock slopes at Palabora Copper Mine, in *Proceedings Seventh Congress of the International Society for Rock Mechanics*, pp 799–804 (International Society for Rock Mechanics: Lisbon).

Eberhardt, E, Woo, K, Stead, D and Elmo, D, 2015. Transitioning from open pit to underground mass mining: meeting the rock engineering challenges of going deeper, in *Proceedings ISRM Congress 2015* (International Society for Rock Mechanics: Lisbon).

Gash, P, 1999. Analysis and interpretation of the *in situ* stress measurements carried out in RAW #1 on the production level, confidential report prepared for Palabora Mining Company.

Glazer, S and Hepworth, N, 2006. Crown pillar failure mechanism – case study based on seismic data from Palabora, *Mass Mining Technology,* 115(2):75–84.

Harrison, J, 2011. Mine subsidence, in *SME Mining Engineering Handbook*, third edition, pp 627–644 (Society for Mining Metallurgy and Exploration: Littleton).

Itasca, 2006. 3DEC. Minneapolis, MN. USA: Itasca Consulting Group.

Itasca, 2015. FLAC3D Version 5.01 Minneapolis, MN USA: Itasca Consulting Group.

Mas Ivars, D, Pierce, M, DeGagné, D and Darcel, C, 2008. Anisotropy and scale dependency in jointed rock mass strength – a synthetic rock mass study, in *Proceedings First International FLAC/DEM Symposium on Numerical Modelling* (eds: R Hart, C Detournay and P Cundall) (Itasca Consulting Group: Minneapolis).

Moss, A, Diachenko, S and Townsend, P, 2006. Interaction between the block cave and the pit slopes at Palabora mine, *The Journal of the South African Institute of Mining and Metallurgy*, 106(7):479–484.

Pretorius, D D and Ngidi, S, 2008. Cave management ensuring optimal life of mine at Palabora, in *Proceedings 5th International Conference and Exhibition on Mass Mining*, pp 63–91 (Luleå University of Technology Press: Luleå).

Rockfield, 2010. ELFEN, Swansea Waterfront, UK.

Sainsbury, B, 2012. A model for cave propagation and subsidence assessment in jointed rock, PhD thesis, School of Mining Engineering, University of New South Wales, Sydney.

Sainsbury, B, Pierce, M and Mas Ivars, D, 2008. Analysis of caving behaviour using a synthetic rock mass – ubiquitous joint rock mass modelling technique, in *Proceedings First Southern Hemisphere International Rock Mechanics Symposium* (eds: Y Potvin, J Carter, A Dyskin and R Jeffrey), pp 243–254 (Australian Centre for Geomechanics: Perth).

Sainsbury, B, Pierce, M and Mas Ivars, D, 2008. Simulation of rock mass strength anisotropy and scale effects using a Ubiquitous Joint Rock Mass (UJRM) model, in *Proceedings First International FLAC/DEM Symposium on Numerical Modelling*, pp 25–27 (Itasca: Minneapolis).

Sainsbury, B and Stockel, B-M, 2012. Large-scale caving and subsidence assessment at the Kiirunavaara Lake Orebody, in *Proceedings Sixth International Conference and Exhibition on Mass Mining (MassMin 2012)*, pp 243–253 (Canadian Institute of Mining, Metallurgy and Petroleum: Montreal).

Sainsbury, D, Lorig, L and Sainsbury, B, 2010. Investigation of caving induced subsidence at the abandoned Grace Mine, in *Proceedings Second International Symposium on Block and Sub-level Caving*, pp 189–204 (Australian Centre for Geomechanics: Perth).

Sainsbury, D, Sainsbury, B and Sweeney, E, in press. Three-dimensional analysis of complex anisotropic slope instability at MMG's Century Mine, *Transactions of the Institutions of Mining and Metallurgy IMM, Mining Technology.*

Singh, M M, 1992. Mine subsidence, in *SME Mining Engineering Handbook* (Society for Mining Metallurgy and Exploration: Littleton).

Vyazmensky, A, Stead, D, Elmo, D and Moss, A, 2010. Numerical analysis of block caving-induced instability in large open pit slopes: a finite element/discrete element approach, *Rock Mechanics and Rock Engineering,* 43(1):21–39.

Woo, K, Eberhardt, E, Rabus, B, Stead, D and Vyazmensky, A, 2012. Integration of field characterisation, mine production and InSAR monitoring data to constrain and calibrate 3-D numerical modelling of block caving-induced subsidence, *International Journal of Rock Mechanics and Mining Sciences*, 53:166–178.